

Optical equilibrium for resonant particles induced by surface plasmons of two-dimensional materials

A. V. Maslov*

University of Nizhny Novgorod, Nizhny Novgorod 603950, Russia

(Received 9 July 2018; revised manuscript received 15 October 2018; published 13 December 2018)

The optomechanical interaction of a resonant particle with a current sheet, graphene for example, induced by its surface plasmon is investigated. It is predicted that stable equilibrium positions for the particle at finite distances from the sheet can be formed. For high-index dielectric particles the equilibria take place in a finite frequency range close to the Mie resonances. Thus, the excitation of resonances by the plasmon and their coupling to the sheet give rise to the strong repulsion, which competes against the usually prevailing attraction induced by the evanescent tail. The formation of purely optical stable equilibria for particles outside of waveguiding structures can find applications for particle propulsion, sorting, and in various systems that require particle isolation.

DOI: [10.1103/PhysRevB.98.235414](https://doi.org/10.1103/PhysRevB.98.235414)

I. INTRODUCTION

The tendency of small dielectric particles to move into the region of the highest intensity of illuminating optical beams and be trapped there forms the foundation of optical tweezing [1]. The optical tweezers have become an indispensable tool of microscience and nanoscience that enables the manipulation of a broad range of objects: microparticles and nanoparticles, biological cells, viruses, atoms, etc. Similar to optical beams, the high-intensity regions inside guiding structures can also trap particles. Trapping and simultaneous propulsion by guided modes was demonstrated for particles inside fiber capillaries [2], hollow-core photonic crystal fibers [3], slot waveguides [4]. Guided modes enable long-range transport of particles due to the lack of diffractive spreading inherent in focused beams. In addition, the use of counterpropagating guided modes allows one to control trapping longitudinally [5,6].

Particles can be trapped and propelled not only inside guiding structures but also outside using the evanescent tails of channel waveguide modes [7,8], surface plasmons [9,10], fiber taper modes [11,12], whispering gallery modes (WGMs) [13], or ring-type resonator modes [14,15]. In all these configurations, the evanescent tails attract the particles to the surface in which proximity other forces may come into play. For example, it is believed that the electrostatic force between the negatively charged gold particles and the negatively surface-charged SiO₂ film is the main mechanism that prevents the gold particles from sticking to the surface [16]. The evanescent tails are particularly useful for creating giant propelling forces on WGM particles. Due to collisions with the fiber the propulsion of large WGM particles is jerky revealing the lack of equilibrium trapping [11,12].

Thus, a key issue in particle manipulation by evanescent tails is the formation of a stable equilibrium in the transverse

direction. The intensity growth with decreasing distance, however, makes the existence of such an equilibrium, at first glance, implausible. The transverse equilibrium in the system consisting of a ring-type resonator evanescently coupled to a waveguide was studied in Ref. [17] where it was shown using a phenomenological theory that there is no stable optical equilibrium in the single-resonance regime. Only in the presence of two resonances a stable equilibrium can appear making it somewhat similar to the stable optical equilibrium for two coupled ring resonators [18]. It was, however, recently shown that a small resonant particle near a metallic surface can be trapped at some distance from it by the optical force induced by the incident plasmon and simultaneously propelled [19]. This purely optical levitation should be distinguished from situations where the optical force counteracts forces of other nature (for example, gravity [20] or mechanical [21]) to form an equilibrium. The purely optical equilibrium position does not depend on the optical power, which defines only the depth of the trapping potential. The possibility to form stable equilibria outside of guiding structures can further facilitate the development of unusual manipulation regimes such as based on negative propelling forces near metals [22,23] or metamaterials [24].

Here it is shown that stable optical equilibria for resonant particles can be formed for a broader range of waveguiding structures compared to that in Ref. [19], namely, for ultrathin layers with in-plane conductivity, i.e., two-dimensional (2D) material. An example of such a waveguiding sheet is graphene, an atomically thin layer of carbon, which has emerged [25] as a promising material for electronic and optical applications [26]. Similar to metals, graphene can support surface plasmons [27–29]. The plasmons in graphene can be tuned by doping or by gating, which opens unprecedented flexibility in developing optoelectronic [30] and optomechanical components. In general, the interaction of polarizable particles with 2D materials differs significantly from that with metal boundaries. Indeed, in the frequency range where surface modes exist, lossless metal (plasma) boundaries

*avmaslov@rf.unn.ru

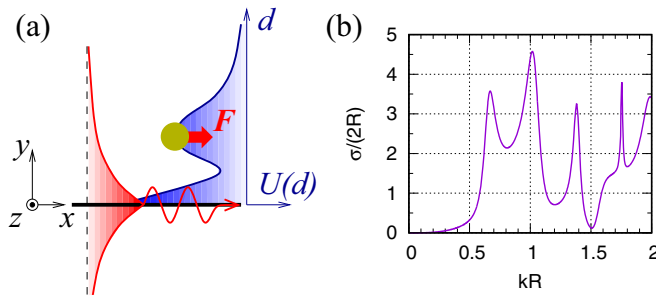


FIG. 1. (a) Schematic of a surface plasmon propagating along a current sheet at $y = 0$ and incident on a particle. The transverse optical potential $U(d)$ has a minimum at some distance from the sheet where the particle can be stably trapped. (b) Normalized scattering cross section for the particle with $\sqrt{\varepsilon} = 3.5$ as a function of the size parameter kR .

provide total reflection for incident plane waves, which surface currents of 2D materials cannot. By the same token, the near field of a dipole at some distance from a 2D material is not described by the simple image dipole as in the case of the half-space boundary. The coupling of nearby emitters to graphene plasmons was studied in Ref. [31]. Similar to the repulsion of particles from the waveguiding boundary due to the coupling to its surface plasmons studied in Ref. [19], the repulsive force on a radiating dipole source near 2D materials can exist [32]. It was also shown in Ref. [32] that if a 2D material lies on a dielectric substrate the combination of the repulsive force and the attractive image-charge force can form an equilibrium for the particle illuminated by a plane wave through the substrate. The presence of equilibrium induced by surface modes, the case addressed in Ref. [19] for the plasmons of a metal boundary and here for the plasmons of 2D materials, demonstrates not only the mere appearance of the repulsive force but also its ability to overcome the attractive force of the evanescent tail that pulls the particle towards the surface in the common geometries of particle propulsion. By solving rigorously the Maxwell equations and accounting for a finite particle size, it is shown here that equilibria can be formed near the particle resonances.

II. PROBLEM FORMULATION AND SOLUTION PROCEDURE

Let us consider a particle with radius R and dielectric permittivity ε separated by a gap d from a generic 2D material, see Fig. 1. The sheet has lateral surface conductivity σ and is assumed to be in vacuum. A plasmon propagates along the sheet and is scattered by the particle. This interaction also creates a force on the particle, which is our primary interest.

We assume 2D geometry in which all properties are invariant in the z direction. The plasmon field defines the transverse magnetic (TM) polarization of the problem with field components $\{H_z, E_x, E_y\}$. The tangential E_x component can be written as

$$E_x(x, y, t) = E_0 e^{ihx - i\omega t - \kappa|y|}, \quad (1)$$

where h is the propagation wave vector, κ is the decay constant. The sheet current in the Drude model is

$$j_x = \sigma E_x, \quad \sigma = ic\Omega/\omega, \quad (2)$$

where Ω is the frequency parameter, which defines the interaction strength (i.e., Drude weight). For graphene, in particular, Eq. (2) for conductivity is valid in a certain frequency range and $\Omega = e^2 E_f / (\pi c \hbar^2)$, where E_f is the Fermi level [33–35]. Collisions are neglected in Eq. (2) for the sake of simplicity. The boundary conditions at the current sheet (2) give the TM plasmon dispersion:

$$h = n_{ph} k, \quad n_{ph} = \sqrt{1 + \omega^2 / (4\pi^2 \Omega^2)}, \quad (3)$$

where n_{ph} is the phase index and $k = \omega/c$. For small frequencies, $\omega/\Omega \ll 1$, the surface plasmon is weakly confined. At high frequencies, $\omega/\Omega \gg 1$, the plasmon becomes strongly confined and that regime is often referred to as quasistatic limit, nonretarded or plasmon approximation [36]. While similar regimes exist for surface plasmons at metal boundaries [37], the properties of surface plasmons of 2D materials also have significant differences. Indeed, the wave number for sheet plasmons (3) grows monotonically with frequency without any cutoffs as long as (2) holds. The cutoff for metal plasmons is related to plasma resonances. The plasma resonances in thin metal films also lead to high reflection for TM waves at bulk plasmon frequency at which the transverse to the film electric field becomes resonantly enhanced [38]. The reflection from sheets does not show any resonances due to the lack of transverse carrier motion. Furthermore, unlike plasma half-space, which gives total reflectivity in the low-frequency region where surface plasmons exist, the reflectivity from sheets is always smaller than unity. Using the boundary conditions across the sheet (2) one obtains the reflection coefficient for H_z of an incident wave $e^{-i\omega t + ihx -igy}$ as

$$r = \xi / (1 + \xi), \quad \xi = 2\pi g \sigma / \omega = i2\pi g c \Omega / \omega^2. \quad (4)$$

The reflectivity $|r|^2$ is maximal at $g = \omega/c$ (normal incidence) and decreases monotonically with decreasing g .

The force is calculated from the fields obtained by solving rigorously the scattering problem. The total field H_z inside the particle is expanded in Bessel functions $J_n(\xi)$ with some unknown coefficients A_n :

$$H_z(\rho < R) = \sum_{n=-\infty}^{\infty} A_n J_n(\sqrt{\varepsilon} k \rho) e^{in\varphi}. \quad (5)$$

This field induces polarization inside, which emits waves propagating towards the sheet. After partial reflection defined by (4) the waves are incident on the particle and generate the total field inside. This forms a set of linear equations for A_n [39]. The force can be calculated using the Lorentz formula describing the mechanical action of the magnetic field on the polarization current and of the electric field on the surface charges. The force components along x (lateral or propelling) and along y (transverse or trapping) can be obtained from A_n [40]. The same formulas can be obtained by inserting the fields just outside the particle into the Maxwell tensor.

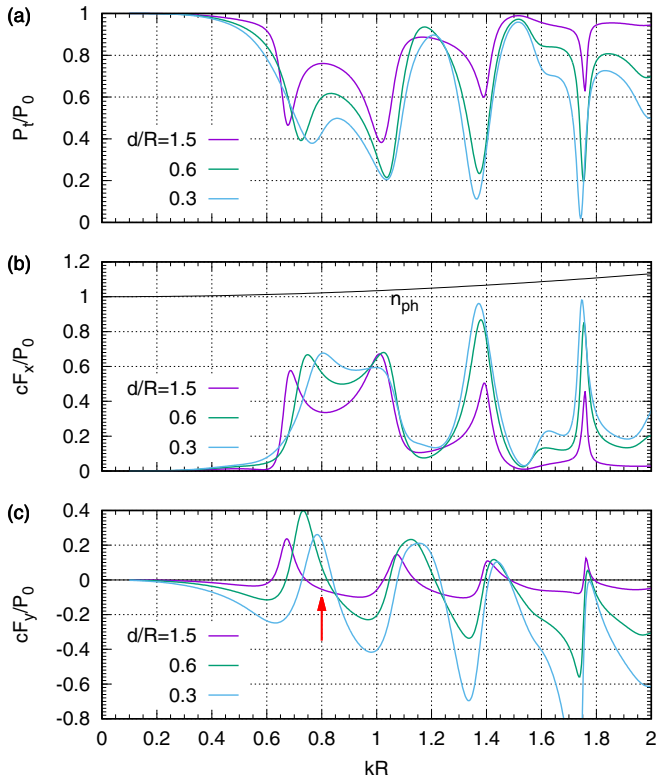


FIG. 2. Frequency dependence of (a) plasmon transmission P_t/P_0 , (b) propelling cF_x/P_0 , and (c) trapping cF_y/P_0 forces on the particle for $\Omega R/c = 0.6$. The arrow in (c) indicates a kR value at which stable transverse equilibrium exists.

III. RESULTS

The scattering cross section for a plane-wave incident on a particle with the refractive index $\sqrt{\varepsilon} = 3.5$ studied in this paper is shown in Fig. 1(b). At low frequencies, $\sqrt{\varepsilon}kR \ll 1$, the scattering cross section grows with kR but remains very small. The peaks describe the excitation of the Mie resonances. The first peak at $kR = 0.67$ describes the lowest (azimuthal number $n = 0$) resonance. This resonance has magnetic type due to the excitation of strong polarization currents and related magnetic field.

The scattering of a graphene plasmon (1) (with power P_0) creates transmitted and reflected plasmons (with powers $P_{t,r}$), as well as bulk radiation (with power P_b) that propagates away from the sheet. Unlike the case of a plasmon guided by metal surface [19], the bulk radiation propagates both in the upper and lower half-spaces towards $y \rightarrow \pm\infty$. Figure 2(a) shows the power of the transmitted plasmon as a function of the frequency parameter kR at fixed values of the relative gap d/R and Drude parameter $\Omega R/c$. The transmission dips correspond to the resonances in Fig. 1(b). In general, the resonant dips broaden and shift with decreasing gap d .

Figures 2(b) and 2(c) show the x and y force components $F_{x,y}$, which are normalized to P_0/c to relate them to the incident plasmon momentum $M_0 = n_{ph}P_0/c$. The propelling F_x becomes strongly enhanced at the transmission dips but remains smaller than M_0 since the transmission is rather high and some momentum is carried by the bulk radiation. The momentum balance was verified in the simulations, i.e., the

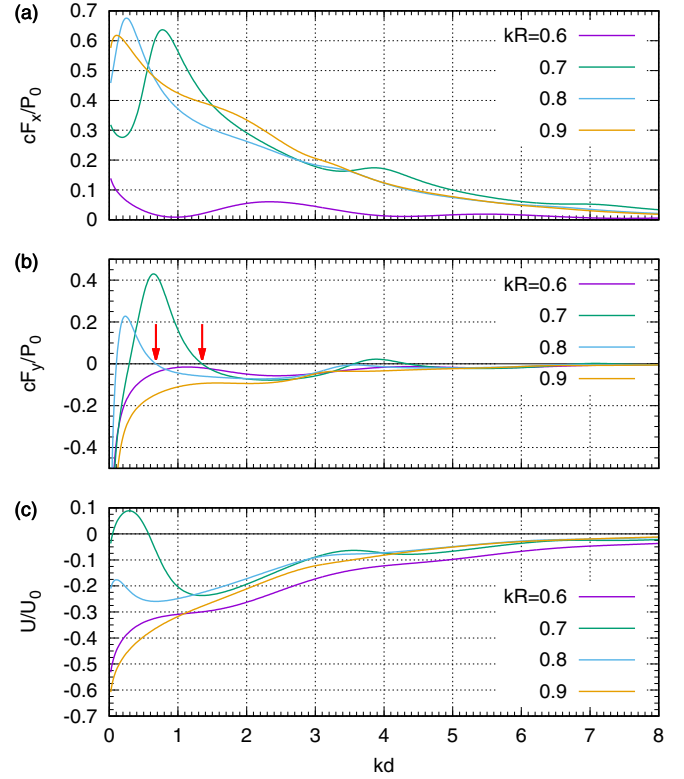


FIG. 3. Gap dependence of (a) propelling cF_x/P_0 , (b) trapping cF_y/P_0 forces, and (c) trapping potential U/U_0 with $U_0 = RP_0/c$ for $\Omega R/c = 0.6$ at several kR . The arrows in (b) indicate the stable equilibria at the smallest gap values d .

difference between the incident electromagnetic momentum and the x component of the final momentum (carried by the two plasmons and bulk waves) is equal to the propelling force on the particle. The transverse F_y in Fig. 2(c) can either attract the particle to the sheet ($F_y < 0$) or repel it ($F_y > 0$). At rather large gaps, $d/R = 1.5$, and outside of resonances, the attractive force pushes the particle to the region of higher field intensity, which reaches maximum at the sheet. At $kR = 0.8$, the attractive force for $d/R = 1.5$ changes to repelling one for $d/R = 0.6$. Thus, there should be a stable equilibrium $F_y = 0$ between these two gap values.

The equilibrium formation can further be investigated by looking at the gap dependence of F_y shown in Figs. 3(b). At $kR = 0.6$ and $kR = 0.9$ the trapping force remains negative for all values of d . In contrast, at $kR = 0.7$ and $kR = 0.8$ the trapping force can be either negative or positive. The gap values at which the trapping force changes sign define the equilibrium positions, which can be either stable or unstable. For example, at $kR = 0.7$, the location $kd = 1.35$ is stable: an increase of d makes F_y negative, which then reduces d ; a decrease of d makes F_y positive, which increases d . In contrast, the equilibrium location $kR = 0.289$ is unstable since any small displacement from it creates a force, which increases it even further. The trapping potential $U(d)$ obtained from $F_y(d)$ is shown in Figs. 3(c). At $kR = 0.7$ and $kR = 0.8$ the potential forms local minima in which the particle can be stably trapped. The particle trapped at the equilibrium position will also be propelled quite efficiently, see Fig. 3(a). Indeed,

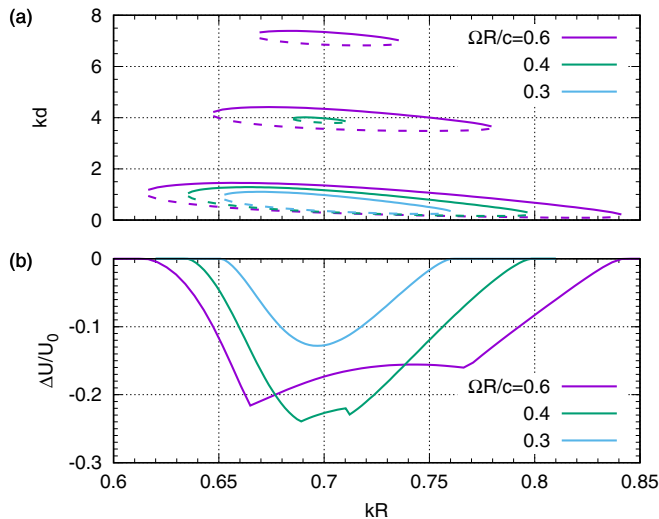


FIG. 4. (a) Stable (solid lines) and unstable (dashed lines) equilibrium positions in the $\{kd, kR\}$ space. (b) Normalized depth of the well with the smallest kd .

at $\Omega R/c = 0.7$, $kR = 1.35$ we obtain a rather high value $cF_x/P_0 = 0.42$. Stronger propulsion, for example $cF_x/P_0 = 0.64$ at $kd = 0.77$, can also be achieved but here the nonzero transverse force will move the particle to the stable position.

Having established the existence of the stable equilibrium, let us now study the parameter range where it exists. Figure 4(a) shows the locations of the equilibrium points $F_y = 0$ at several values of $\Omega R/c$. The points always lie near the resonance, $0.6 \lesssim kR \lesssim 0.85$. For the weaker confined plasmon, $\Omega R/c = 0.6$, there can be up to three stable and three unstable equilibrium points depending on kR . The stable location at the lowest kd is characterized by the strongest trapping, i.e., deepest potential well, see Fig. 3(c). The trapping strength for higher kd is very weak. Also the frequency range (or particle size range) kR at which stable trapping can be realized decreases for larger gaps corresponding to weakening of the particle-sheet interaction. This decrease in the interaction strength also gives smaller ranges of trapping parameters for the stronger confined plasmons with $\Omega R/c = 0.4, 0.3$.

Figure 4(b) shows the depth of the well with the smallest kd , which is defined as the energy difference between the bottom of the well and the lowest (left or right) barrier, see also Fig. 3(c). The depth, in general, shows quite complicated behavior. At $\Omega R/c = 0.6$, the well starts to be formed at $kR \approx 0.61$ and becomes initially deeper with increasing kR . Then at $kR \approx 0.665$ its depth starts to decrease. The jump in the derivative is related to the fact that at $kR < 0.665$ the depth was defined by the barrier on the left, while at $kR > 0.665$, by the barrier on the right. The reverse switch takes place at $kR \approx 0.767$. For $\Omega R/c = 0.4$ we observe a similar behavior except that at $kR = 0.711$ there is a jump, which is related to the disappearance of the neighboring well at higher kd . At $\Omega R/c = 0.3$ the depth function is smooth, with a well-defined minimum. Among the three values $\Omega R/c = 0.3, 0.4, 0.6$, the deepest well $\Delta U/U_0 = -0.239$ is obtained for the intermediate value $\Omega R/c = 0.4$ at $kR = 0.689$.

To verify the analytical predictions, finite-difference time-domain (FDTD) simulations were performed using an in-

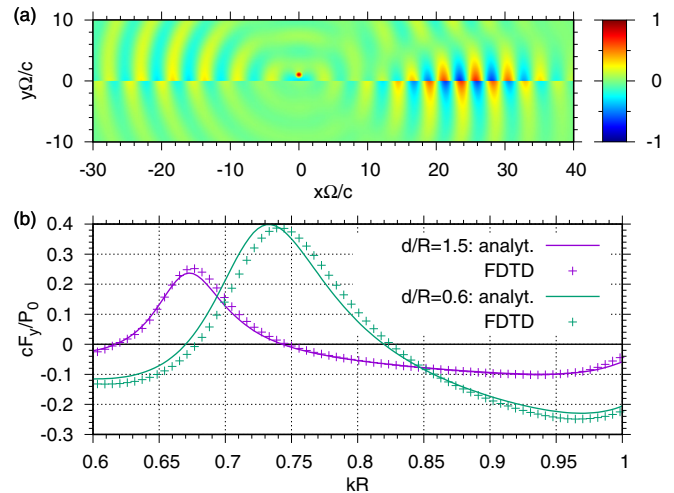


FIG. 5. (a) Snapshot of $H_z(x, y)$ created by the incident plasmon wave packet at some moment after it passes the particle located at $x = 0$. The size of the particle was $R\Omega/c = 0.6$. (b) Comparison of transverse forces cF_y/P_0 calculated analytically and using the FDTD method.

house developed code. The simulations describe the time evolution of the fields originating from an initially created plasmon wave packet propagating towards the scattering particle. A typical snapshot of $H_z(x, y)$ in Fig. 5 shows the formation of the reflected plasmon at $x < 0$, transmitted plasmon at $x > 0$ as well as bulk radiation. The fields in the frequency domain were calculated at a box around the particle and subsequently used to find the force using the Maxwell tensor. The forces calculated by the analytical and FDTD methods for two different gap values $d/R = 1.5, 0.6$ agree very well, see Fig. 5(b). The small difference can be attributed to a finite size of the FDTD cell, which introduces discretization errors. From Fig. 5(b) one can also deduce the existence of stable equilibrium in the parameter range at least $0.75 < kR < 0.82$, where the attractive force at $d/R = 1.5$ changes to repelling at $d/R = 0.6$.

The use of normalization allows one to estimate forces for given power. Let us assume that the guided power incident on the particle is 0.3 mW and the normalized force is $cF_y/P_0 \sim 0.1$. The actual force becomes $F_y \sim 0.1$ pN. The force magnitude can be directly controlled by changing incident power.

IV. CONCLUSION

To conclude, it has been shown that a resonant particle near a current sheet, such as graphene, can be trapped by the surface plasmon at some specific distance from the sheet. The appearance of stable trapping outside of the guiding structure results from the strong interaction of the resonantly excited particle with the sheet since in its absence the evanescent tail of the plasmon would merely bring the particle in contact with the sheet. The predictions are based on analytical and FDTD approaches to the scattering problem in 2D, which account rigorously for the strong particle-sheet interactions at subwavelength gaps. The stable trapping may enable the further development of optomechanical technologies related

to transport [41], manipulation, and isolation of particles from the environment [42] and graphene plasmonics [26].

Similar to propagating modes, localized resonances also attract particles into the high-intensity regions and, unlike propagating modes, immobilize them. Examples include voids in metal films [43–45] and metal pads [46,47]. The trapping inside cavities can lead to the changes in the resonant frequencies and trapping efficiency [45,48,49]. Similar to voids in metals, localized plasmons of apertures in graphene can attract particles to the aperture edges [50]. One can expect that the formation of stable equilibria at finite distances from the surface demonstrated here for propagating plasmons exists for localized plasmons as well.

Besides the trapping of dielectric particles, one can also envision the trapping of atoms, molecules, and ions required

for the creation of hybrid devices consisting of atomic and solid-state subsystems. In particular, atoms can be trapped near a sharp metallic tips [51] or an an aperture of the scanning near-field optical microscope tip [52] and then coupled to other structures (such as resonators) or to surface plasmons of the tip. Unlike these schemes that create the trapping potential by some incident field [51,52], the trapping described here emerges only as the result of the interaction between the resonant particle and the waveguiding structure.

ACKNOWLEDGMENT

The author is grateful to the anonymous referees for bringing Ref. [32] to his attention.

-
- [1] A. Ashkin, *Phys. Rev. Lett.* **24**, 156 (1970).
- [2] M. J. Renn, R. Pastel, and H. J. Lewandowski, *Phys. Rev. Lett.* **82**, 1574 (1999).
- [3] F. Benabid, J. C. Knight, and P. S. J. Russell, *Opt. Express* **10**, 1195 (2002).
- [4] A. H. J. Yang, S. D. Moore, B. S. Schmidt, M. Klug, M. Lipson, and D. Erickson, *Nature (London)* **457**, 71 (2009).
- [5] D. S. Bykov, O. A. Schmidt, T. G. Euser, and P. S. J. Russell, *Nature Photon.* **9**, 461 (2015).
- [6] M. Daly, V. G. Truong, and S. N. Chormaic, *Opt. Express* **24**, 14470 (2016).
- [7] S. Kawata and T. Tani, *Opt. Lett.* **21**, 1768 (1996).
- [8] H. Jaising and O. Hellesø, *Opt. Commun.* **246**, 373 (2005).
- [9] V. Garcés-Chávez, G. C. Spalding, and K. Dholakia, *Proc. SPIE* **5930**, 59301B (2005).
- [10] G. Volpe, R. Quidant, G. Badenes, and D. Petrov, *Phys. Rev. Lett.* **96**, 238101 (2006).
- [11] Y. Li, O. V. Svitelskiy, A. V. Maslov, D. Carnegie, E. Rafailov, and V. N. Astratov, *Light: Sci. Appl.* **2**, e64 (2013).
- [12] Y. Li, A. V. Maslov, N. I. Limberopoulos, A. M. Urbas, and V. N. Astratov, *Laser Photon. Rev.* **9**, 263 (2015).
- [13] S. Arnold, D. Keng, S. I. Shopova, S. Holler, W. Zurawsky, and F. Vollmer, *Opt. Express* **17**, 6230 (2009).
- [14] S. Mandal, X. Serey, and D. Erickson, *Nano Lett.* **10**, 99 (2010).
- [15] S. Lin, E. Schonbrun, and K. Crozier, *Nano Lett.* **10**, 2408 (2010).
- [16] K. Wang, E. Schonbrun, and K. B. Crozier, *Nano Lett.* **9**, 2623 (2009).
- [17] V. Intaraprasong and S. Fan, *Opt. Express* **21**, 25257 (2013).
- [18] P. Rakich, M. Popović, M. Soljačić, and E. P. Ippen, *Nature Photon.* **1**, 658 (2007).
- [19] A. V. Maslov, *Opt. Lett.* **42**, 3327 (2017).
- [20] A. Ashkin and J. M. Dziedzic, *Appl. Phys. Lett.* **19**, 283 (1971).
- [21] M. Eichenfield, C. P. Michael, R. Perahia, and O. Painter, *Nature Photon.* **1**, 416 (2007).
- [22] A. V. Maslov, *Phys. Rev. Lett.* **112**, 113903 (2014).
- [23] M. I. Petrov, S. V. Sukhov, A. A. Bogdanov, A. S. Shalin, and A. Dogariu, *Laser Photon. Rev.* **10**, 116 (2016).
- [24] I. Nefedov and A. S. Shalin, *Physica Status Solidi Rapid Res. Lett.* **11**, 1700219 (2017).
- [25] K. S. Novoselov, A. K. Geim, S. V. Morozov, D. Jiang, Y. Zhang, S. V. Dubonos, I. V. Grigorieva, and A. A. Firsov, *Science* **306**, 666 (2004).
- [26] A. N. Grigorenko, M. Polini, and K. S. Novoselov, *Nature Photonics* **6**, 749 (2012).
- [27] J. Chen, M. Badioli, P. Alonso-González, S. Thongrattanasiri, F. Huth, J. Osmond, M. Spasenović, A. Centeno, A. Pesquera, N. Camara, F. J. G. de Abajo, R. Hillenbrand, and F. H. L. Koppens, *Nature (London)* **487**, 77 (2012).
- [28] Z. Fei, A. S. Rodin, G. O. Andreev, W. Bao, A. S. McLeod, M. Wagner, L. M. Zhang, Z. Zhao, M. Thiemens, G. Dominguez, M. M. Fogler, A. H. C. Neto, C. N. Lau, F. Keilmann, and D. N. Basov, *Nature (London)* **487**, 82 (2012).
- [29] X. Lin, I. Kaminer, X. Shi, F. Gao, Z. Yang, Z. Gao, H. Buljan, J. D. Joannopoulos, M. Soljačić, H. Chen, and B. Zhang *Sci. Adv.* **3**, e1601192 (2017).
- [30] F. J. García de Abajo, *ACS Photon.* **1**, 135 (2014).
- [31] F. H. L. Koppens, D. E. Chang, and F. J. García de Abajo, *Nano Lett.* **11**, 3370 (2011).
- [32] F. J. Rodríguez-Fortuño, M. F. Picardi, and A. V. Zayats, *Phys. Rev. B* **97**, 205401 (2018).
- [33] P. R. Wallace, *Phys. Rev.* **71**, 622 (1947).
- [34] G. W. Hanson, *J. Appl. Phys.* **103**, 064302 (2008).
- [35] M. Jablan, H. Buljan, and M. Soljačić, *Phys. Rev. B* **80**, 245435 (2009).
- [36] Y. V. Bludov, A. Ferreira, N. M. R. Peres, and M. I. Vasilevskiy, *Int. J. Mod. Phys. B* **27**, 1341001 (2013).
- [37] R. Ritchie, *Surf. Sci.* **34**, 1 (1973).
- [38] R. A. Ferrell, *Phys. Rev.* **111**, 1214 (1958).
- [39] A. V. Maslov, *IEEE Trans. Antennas Propag.* **66**, 2904 (2018).
- [40] A. V. Maslov, V. N. Astratov, and M. I. Bakunov, *Phys. Rev. A* **87**, 053848 (2013).
- [41] D. Erickson, X. Serey, Y.-F. Chenac, and S. Mandal, *Lab on Chip* **11**, 995 (2011).
- [42] M. Bhattacharya, A. N. Vamivakas, and P. Barker, *J. Opt. Soc. Am. B* **34**, L01 (2017).
- [43] R. Sainidou and F. J. García de Abajo, *Phys. Rev. Lett.* **101**, 136802 (2008).
- [44] M. L. Juan, R. Gordon, Y. Pang, F. Eftekhari, and R. Quidant, *Nature Phys.* **5**, 915 (2005).

- [45] M. L. Juan, M. Righini, and R. Quidant, *Nature Photon.* **5**, 349 (2011).
- [46] M. Righini, C. Girard, and R. Quidant, *J. Opt. A: Pure Appl. Opt.* **10**, 093001 (2008).
- [47] H. M. K. Wong, M. Righini, J. C. Gates, P. G. R. Smith, V. Pruneri, and R. Quidant, *Appl. Phys. Lett.* **99**, 061107 (2011).
- [48] N. Descharmes, U. P. Dharanipathy, Z. Diao, M. Tonin, and R. Houdre, *Phys. Rev. Lett.* **110**, 123601 (2013).
- [49] P. Mestres, J. Berthelot, S. S. Aćimović, and R. Quidant, *Light: Sci. Appl.* **5**, e16092 (2016).
- [50] J. Zhang, W. Liu, Z. Zhu, X. Yuan, and S. Qin, *Sci. Rep.* **6**, 38086 (2016).
- [51] D. E. Chang, J. D. Thompson, H. Park, V. Vuletić, A. S. Zibrov, P. Zoller, and M. D. Lukin, *Phys. Rev. Lett.* **103**, 123004 (2009).
- [52] V. Klimov, S. Sekatskii, and G. Dietler, *Opt. Commun.* **259**, 883 (2006).